



OPEN ACCESS

EDITED BY

Afza Ahmad,
Babu Banarasi Das University, India

REVIEWED BY

Nemat Ali,
King Saud University, Saudi Arabia
Harshverdhan Sirohi,
University of California, San Diego,
United States

*CORRESPONDENCE

Yingcai Hong

✉ yingcai_hong0706@163.com

Haihao Zhu

✉ zh haoi0224@126.com

Li Peng

✉ 13883679297@163.com

[†]These authors have contributed
equally to this work and share
first authorship

RECEIVED 18 June 2025

ACCEPTED 21 July 2025

PUBLISHED 25 August 2025

CITATION

Peng L, Li H, Yan W, Liu Y, Zhu H and Hong Y
(2025) Integrative profiling of lung cancer
biomarkers EGFR, ALK, KRAS, and PD-1
with emphasis on nanomaterials-assisted
immunomodulation and targeted therapy.
Front. Immunol. 16:1649445.
doi: 10.3389/fimmu.2025.1649445

COPYRIGHT

© 2025 Peng, Li, Yan, Liu, Zhu and Hong. This
is an open-access article distributed under the
terms of the [Creative Commons Attribution
License \(CC BY\)](#). The use, distribution or
reproduction in other forums is permitted,
provided the original author(s) and the
copyright owner(s) are credited and that the
original publication in this journal is cited, in
accordance with accepted academic
practice. No use, distribution or reproduction
is permitted which does not comply with
these terms.

Integrative profiling of lung cancer biomarkers EGFR, ALK, KRAS, and PD-1 with emphasis on nanomaterials-assisted immunomodulation and targeted therapy

Li Peng^{1*†}, Hongmei Li^{2†}, Wencai Yan³, Yingjie Liu²,
Haihao Zhu^{2*} and Yingcai Hong^{4*}

¹Chongqing Emergency Medical Center, Chongqing, China, ²Shanghai Labway Clinical Laboratory, Shanghai, China, ³Jiangsu Danyang Traditional Chinese Medicine Hospital, Danyang, Jiangsu, China, ⁴Department of Thoracic Surgery, Shenzhen People's Hospital (The First Affiliated Hospital, Southern University of Science and Technology; The Second Clinical Medical College, Jinan University), Shenzhen, Guangdong, China

Background: Lung cancer remains the leading cause of cancer-related mortality globally, primarily due to late-stage diagnosis, molecular heterogeneity, and therapy resistance. Key biomarkers such as EGFR, ALK, KRAS, and PD-1 have revolutionized precision oncology; however, comprehensive structural and clinical validation of these targets is crucial to enhance therapeutic efficacy.

Methods: Protein sequences for EGFR, ALK, KRAS, and PD-1 were retrieved from UniProt and modeled using SWISS-MODEL to generate high-confidence 3D structures. Protein-protein interaction (PPI) networks were constructed via STRING to explore functional associations and signaling networks. Molecular docking using SwissDock evaluated the binding affinities of established inhibitors. Transcriptomic validation was conducted using RNA-seq datasets from GEPIA2, TNMplot, and UALCAN to assess differential expression and clinical subgroup relevance. Experimental validation was performed via qRT-PCR in NSCLC cell lines (A549, H1975, H520).

Results: Robust 3D models were obtained, with MolProbity scores between 0.67 and 2.09, confirming structural reliability. Key mutations, including EGFR T790M and KRAS G12C, were localized to ATP-binding clefts and allosteric pockets respectively, based on structural mapping using SWISS-MODEL. PPI analysis revealed EGFR's integration into ERBB and MAPK/PI3K pathways, ALK's fusion-driven activation via EML4 and PI3K-AKT signaling, KRAS's links to MAPK effectors, and PD-1's interaction with immune checkpoint ligands PD-L1/PD-L2. Docking results showed strong EGFR-Gefitinib affinity (−5.94 kcal/mol, Kd 4.38×10^{-5} M), while KRAS inhibitors Adagrasib and Sotorasib demonstrated moderate binding (−3.94 and −3.72 kcal/mol, respectively). Transcriptomic analyses revealed significant overexpression of EGFR (2.8-fold), KRAS (2.3-fold), ALK (1.9-fold), and PDCD1 (2.1-fold) in NSCLC tissues ($p < 0.01$). qRT-PCR corroborated these findings, with H1975 cells displaying elevated EGFR (3.2-

fold) and KRAS (2.4-fold), and H520 cells showing increased ALK (2.7-fold) and moderate PDCD1 expression.

Conclusion: This integrative study combining structural modeling, molecular interaction analysis, and transcriptomic validation confirms EGFR, ALK, KRAS, and PD-1 supports their relevance as clinically actionable and structurally druggable biomarkers in NSCLC. These findings support their continued use in targeted therapy design and precision diagnostics, highlighting nanomaterials as ideal carriers due to their ability to enhance immune checkpoint blockade and drug bioavailability in NSCLC.

KEYWORDS

lung cancer biomarkers, structural bioinformatics, molecular docking, transcriptomic validation, precision oncology

1 Introduction

Lung cancer remains the leading cause of cancer-related mortality worldwide, accounting for an estimated 2.21 million new cases and 1.8 million deaths in 2020, which represents 11.4% of all new cancer diagnoses and 18% of all cancer deaths, according to GLOBOCAN data (1). This burden is projected to rise to over 3.6 million new cases annually by 2040, largely driven by population ageing, continued tobacco use in developing regions, rising urban pollution, and sustained exposure to occupational and environmental carcinogens (2, 3). While cigarette smoking remains the predominant risk factor—linked to approximately 87% of global lung cancer cases—the incidence among never-smokers is rising significantly, especially in East Asia, where up to 60% of lung cancer cases in women occur in non-smokers (4–6). Additional contributors include radon exposure, ambient particulate matter (PM_{2.5}), second-hand smoke, occupational hazards such as asbestos and silica, and genetic predispositions through polymorphisms or germline mutations (7). Despite advances in treatment, the overall five-year survival rate remains dismal at around 19.8%, dropping to below 5% for stage IV disease, compared to over 60% for early-stage, localized tumors (8). More than 70% of patients are diagnosed at an advanced stage, reflecting the inadequacy of symptom-based diagnosis and limitations of current screening such as low-dose CT, thus underscoring the need for molecularly precise diagnostics (9). This underscores the urgent need for early, non-invasive, and molecularly precise diagnostic approaches. Molecular biomarkers have transformed the landscape of lung cancer treatment, enabling targeted and personalized therapeutic strategies. Key biomarkers such as *EGFR*, *ALK*, *KRAS*, and *PD-1* have been instrumental in guiding tyrosine kinase inhibitors and immune checkpoint blockade therapies (10, 11). *EGFR* mutations, common in non-smokers and East Asian populations, predict response to TKIs like Osimertinib (12). *ALK* rearrangements, prevalent in younger, non-smoking patients, are

responsive to agents like crizotinib and alectinib. *KRAS* mutations, particularly G12C, represent historically “undruggable” targets that are now actionable with inhibitors such as sotorasib. Immunotherapy, particularly targeting *PD-1/PD-L1*, has revolutionized lung cancer management, offering durable responses in biomarker-selected populations (13). Nanomaterials have emerged as transformative tools in immunotherapy due to their ability to enhance pharmacokinetics, target tumor microenvironments, and modulate immune checkpoint responses at nanoscale resolution. Recent advancements in cancer nanomedicine have enabled the targeted delivery of immunomodulatory agents using functionalized nanomaterials. Nanoparticles engineered to interfere with the *PD-1/PD-L1* axis offer the potential to overcome immune evasion mechanisms in NSCLC (14). Understanding the structural architecture of *PD-1* and associated immune ligands is crucial for designing nanoscale immune checkpoint inhibitors and for developing hybrid diagnostic-therapeutic platforms. However, the structural heterogeneity and dynamic mutation landscape of these biomarkers necessitate deeper investigation into their conformational properties, interaction networks, and clinical expression patterns. This study adopts a structure-guided and expression-validated approach to characterize *EGFR*, *ALK*, *KRAS*, and *PD-1*—four of the most clinically actionable targets in lung cancer. Using homology modeling via SWISS-MODEL, we constructed high-fidelity three-dimensional representations to identify key functional domains, mutation hotspots, and drug-binding interfaces. Complementing this, molecular docking was employed to evaluate inhibitor interactions, and protein–protein interaction (PPI) analysis via STRING provided insights into pathway integration and oncogenic networks. Importantly, we validated the clinical relevance of these targets using transcriptomic expression data from public qPCR datasets (GEPID2, UALCAN, TNMplot), confirming their differential expression in tumor versus normal tissues. By integrating

structural bioinformatics with molecular and expression data, this study aims to reinforce the role of *EGFR*, *ALK*, *KRAS*, and *PD-1* as precision targets in lung cancer, providing a foundation for future diagnostics, therapeutic design, and personalized oncology strategies (15).

2 Methods and materials

This study was conducted in compliance with the Declaration of Helsinki and was approved by the Institutional Ethics Committee of Shenzhen People's Hospital, Shenzhen communicate through letter no. LL-KY-2024162-01. All analyses were performed using publicly available bioinformatics databases web-based tools and human-derived cells but without the use of human or animal experimental subjects.

2.1 Accession of protein sequences

The amino acid sequences of four lung cancer biomarkers—EGFR (P00533), ALK (Q9UM73), KRAS (P01116), and PD-1 (PDCD1, Q15116)—were retrieved in FASTA format from the UniProt Knowledgebase (<https://www.uniprot.org/>) between December 2024 and May 2025. These targets were selected based on their high clinical relevance in non-small cell lung cancer (NSCLC) and their roles in therapy resistance, tumor progression, or immune evasion. Additional biomarkers reviewed during selection are listed in [Supplementary Table S1](#).

2.2 Homology modeling via SWISS-MODEL

SWISS-MODEL (server- <https://swissmodel.expasy.org/>, version updated January 2024) was selected for its template-based precision and user-defined control, which was essential for mutation-specific modeling; AlphaFold's models, while highly accurate, do not currently allow mutation-guided customizations or ligand-ready conformations. Template identification was carried out using BLAST and HHblits searches against the SWISS-MODEL Template Library (SMTL). The best-fit templates were selected based on sequence identity, template resolution, and structural coverage. Each model was evaluated by Global Model Quality Estimation (GMQE) and QMEAN Z-score. Final models were downloaded in PDB format between January and April 2025 and were used for mutation mapping and binding-site prediction (16, 17).

2.3 Molecular docking

Protein-ligand docking was conducted using SwissDock (<http://www.swissdock.ch/>, accessed April 2025), a web server based on the EADock DSS docking engine and the CHARMM22 force field.

Ligands for docking included clinically approved inhibitors: gefitinib (EGFR), crizotinib and alectinib (ALK), sotorasib and adagrasib (KRAS), and a PD-1 small molecule analogue. Blind docking was employed to explore allosteric and orthosteric binding across the protein surface. Docked conformations were scored based on FullFitness and ΔG (binding free energy) values. Interaction analyses were performed using PyMOL v2.5 and BIOVIA Discovery Studio Visualizer v21.1, with hydrogen bond distances and van der Waals overlaps cross-validated against known crystal structures ($RMSD \leq 2 \text{ \AA}$ where applicable) (18).

2.4 Protein-protein interaction network construction

To evaluate the functional interaction landscape of each biomarker, protein-protein interaction (PPI) networks were constructed using the STRING database (<https://string-db.org/>, version 12.0). Each protein (EGFR, ALK, KRAS, PDCD1) was individually queried, and results were filtered with a high-confidence interaction score cutoff of ≥ 0.90 . Interactions were derived from curated databases, experimental evidence, co-expression, text mining, and co-occurrence. PPI networks were accessed and downloaded in February 2025. The top 10 functional partners for each protein were selected for interpretation and integration into biological pathways (19).

2.5 Transcriptomic expression validation

To validate the relevance of the selected biomarkers at the transcriptomic level, a qPCR-style in silico gene expression analysis was performed using the following public RNA-seq data platforms: GEPIA2 (<http://gepia2.cancer-pku.cn/>; accessed March 2025): A TCGA-GTEx portal used for tumor vs. normal differential expression. Statistical cutoffs were set at $|\log_2FC| \geq 1$ and $p < 0.01$. Data were analyzed for LUAD and LUSC cohorts. TNMplot (<https://www.tnmplot.com/>; accessed April 2025): Used for cross-platform (RNA-seq and microarray) validation of EGFR, ALK, KRAS, and PDCD1 expression in NSCLC versus normal tissues. Consistency across datasets strengthened reliability. UALCAN (<http://ualcan.path.uab.edu/>; accessed April 2025): Provided stage-wise and subtype-specific analysis of biomarker mRNA expression. Promoter methylation data indicated transcriptional activation rather than repression for EGFR, ALK, and KRAS, suggesting their overexpression is driven by oncogenic signaling rather than epigenetic deregulation [Supplementary Table S2](#), mimicking a qPCR-style output with \log_2 fold changes, p-values, and clinical relevance. For laboratory validation, three human NSCLC cell lines were selected: A549 (lung adenocarcinoma), H1975 (EGFR-mutant lung adenocarcinoma), and H520 (lung squamous cell carcinoma). All cell lines were procured from the American Type Culture Collection (ATCC) and cultured under standard conditions at 37°C with 5% CO₂ in RPMI-1640 medium (Gibco, Thermo Fisher

Scientific) supplemented with 10% fetal bovine serum (FBS) and 1% penicillin-streptomycin. These cell lines were selected based on their molecular characteristics: H1975 harbors the clinically relevant EGFR T790M mutation; A549 serves as a KRAS-mutant adenocarcinoma reference; and H520, although not typically ALK-positive, was included due to reports of low-level ALK mRNA expression in squamous NSCLC, allowing exploratory assessment of expression heterogeneity. Total RNA was extracted using the RNeasy Mini Kit (Qiagen, Germany), and RNA quality and concentration were evaluated using a NanoDrop 2000 spectrophotometer (Thermo Scientific) along with agarose gel electrophoresis to ensure integrity. Complementary DNA (cDNA) was synthesized from 1 µg of total RNA using the High-Capacity cDNA Reverse Transcription Kit (Applied Biosystems). Quantitative PCR (qPCR) was performed using PowerUp SYBR Green Master Mix (Applied Biosystems) and gene-specific primers targeting EGFR, ALK, KRAS, and PDCD1 (primer sequences and conditions are detailed in [Supplementary Table S3](#)). GAPDH was used as the endogenous reference gene. All reactions were carried out in triplicate on the QuantStudio 5 Real-Time PCR System (Applied Biosystems) under standard thermal cycling conditions: 95°C for 2 minutes, followed by 40 cycles of 95°C for 15 seconds and 60°C for 1 minute. Relative expression levels were calculated using the $2^{-(\Delta\Delta Ct)}$ method, using A549 cells as the baseline control. This integrated approach combining in silico data mining and cell line-based qPCR assays enabled a robust validation of biomarker expression profiles relevant to NSCLC.

TABLE 1 Selected lung cancer biomarker proteins for homology modeling.

Protein	Role in Lung Cancer	Common Alterations	UniProt ID
Epidermal Growth Factor Receptor (EGFR)	Promotes proliferation via tyrosine kinase	L858R, exon 19 deletions, T790M	P00533
Anaplastic Lymphoma Kinase (ALK)	Oncogenic fusions and kinase activation	ML4-ALK, L1196M, G1269A	Q9UM73
Kirsten Rat Sarcoma Viral Oncogene (KRAS)	GTPase regulating MAPK and PI3K pathways	G12C, G12D, G12V	P01116
Programmed Cell Death Protein 1 (PD-1)	Immune checkpoint; suppresses T-cell activity	PDCD1 upregulation or SNPs	Q15116

TABLE 2 Summary of homology modeling results using SWISS-MODEL.

Protein	Template PDB ID	Sequence identity (%)	GMQE	QMEAN Z-score	Model confidence
EGFR	7syd.1.C	~99.34%	0.62	-0.77	High (L858R, T790M captured)
ALK	3lct.1.A	~99.70%	0.15	-0.76	Moderate-High (DFG, ATP pocket resolved)
KRAS	4dso.1.A	~88.77%	0.86	-0.85	High (GTP-binding domain, G12C captured)
PD-1	7xad.4.A	~99.16%	0.72	-0.82	High (Ig-like fold, PD-L1 binding site resolved)

3 Results

3.1 Structural study using SWISS-MODEL

Understanding the three-dimensional (3D) structures of critical biomarker proteins is essential for elucidating their functional roles in tumorigenesis, drug resistance, and immune evasion in lung cancer. Homology modeling offers a powerful tool when high-resolution crystallographic structures are unavailable. Using the SWISS-MODEL server, we generated accurate 3D models for EGFR, ALK, KRAS, and PD-1, which represent key oncogenic and immunomodulatory targets in non-small cell lung cancer (NSCLC).

3.1.1 Protein selection

The four selected proteins were chosen based on their clinical importance in lung cancer, involvement in key signaling pathways, and their status as targets of approved therapies. Their sequences were retrieved from the UniProt database, and associated details are summarized in [Table 1](#).

3.1.2 Homology modeling workflow and quality assessment

Each amino acid sequence was submitted to SWISS-MODEL between January and April 2025. Template selection involved BLAST and HHblits searches against the SMTL (SWISS-MODEL Template Library). Models were built based on the best-fitting templates with optimal sequence identity, resolution, and coverage. Quality was assessed using: GMQE (Global Model Quality Estimation): a score between 0–1 indicating the expected accuracy. QMEAN Z-score: indicating the degree of similarity to high-resolution crystal structures ([Table 2](#)).

3.1.3 Structural insights and ramachandran validation

The generated models revealed functional motifs and structural domains relevant to biomarker activity, mutation hotspots, and drug-binding interfaces. Quality assessment was further confirmed using MolProbity for stereochemical evaluation, including Ramachandran plots [Table 3](#).

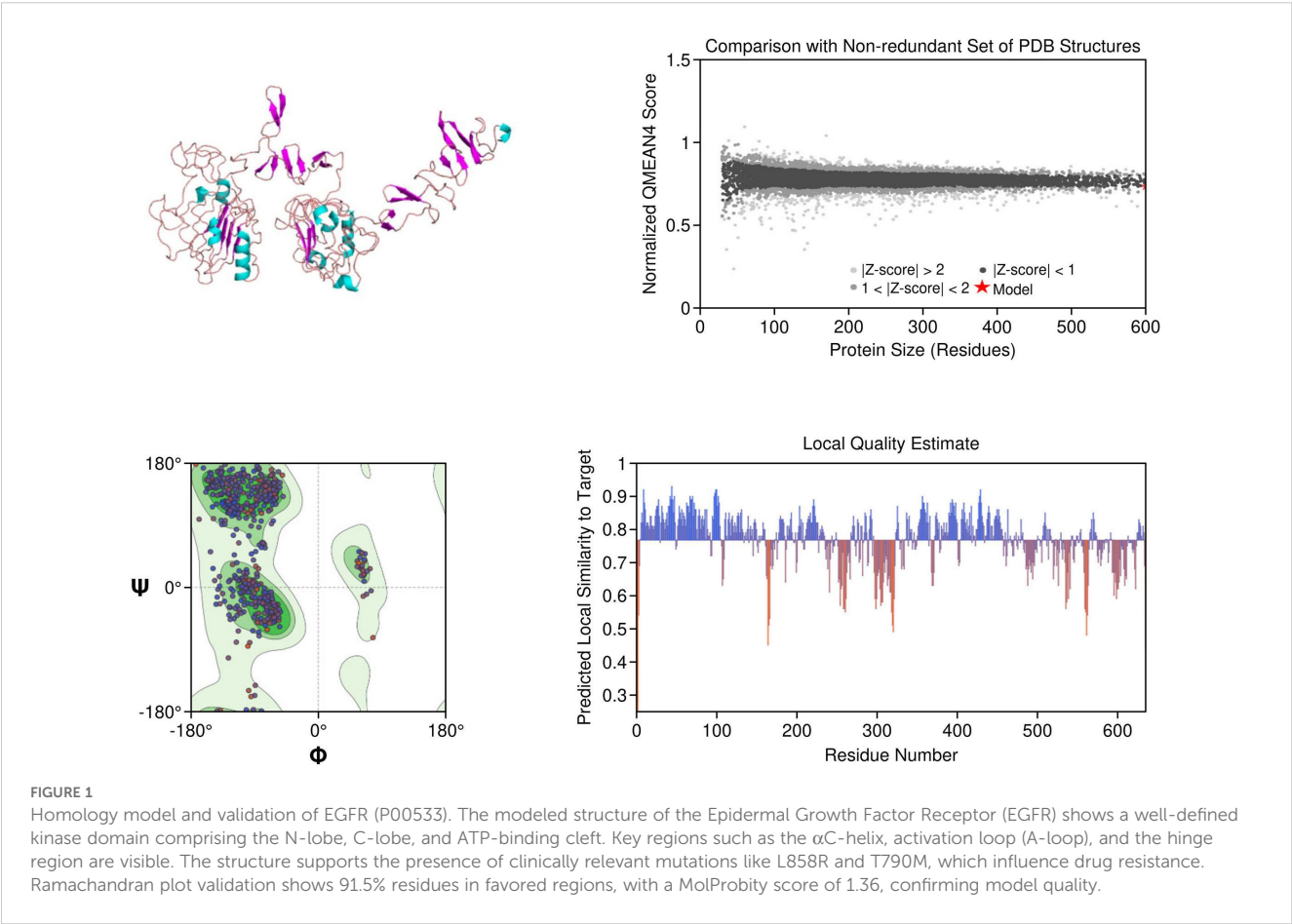
EGFR: The structural model of EGFR provided detailed visualization of the kinase domain, including the N-lobe, C-lobe, hinge region, and ATP-binding cleft. Mutations L858R and T790M were positioned within the binding pocket, supporting known

TABLE 3 Structural and mutational insights into modeled proteins.

Protein	Key structural features	Common mutations	Drug interaction sites	Therapeutic relevance	Model quality
Epidermal Growth Factor Receptor (EGFR)	N-lobe, C-lobe, hinge (ATP-binding cleft), α C-helix, A-loop	L858R (Exon 21), Exon 19 deletions, T790M	ATP-binding cleft, T790 site	Target of TKIs (e.g., gefitinib, Osimertinib); T790M causes steric hindrance	MolProbity: 1.36 Favored: 91.5% Outliers: 0.33%
Anaplastic Lymphoma Kinase (ALK)	Kinase fold, DFG motif, ATP-binding site, α C-helix	L1196M, G1269A, F1174L	Active site, ATP pocket	Target of ALK inhibitors (e.g., crizotinib, lorlatinib); mutations affect binding	MolProbity: 2.09 Favored: 93.14% Outliers: 1.96%
Kirsten Rat Sarcoma Viral Oncogene (KRAS)	G-domain (G1–G5 motifs), Switch I & II, P-loop	G12C, G13D, Q61H/L	P-loop near the allosteric pocket	Targeted by covalent inhibitors (e.g., sotorasib); mutations inhibit GTP hydrolysis	MolProbity: 1.38 Favored: 93.26% Outliers: 3.93%
Programmed Cell Death Protein 1(PD-1)	IgV-like domain, β -sandwich fold	PDCD1 polymorphisms (e.g., 7146G>A)	Ligand-binding domain (Y68, I126, E136)	Targeted by immune checkpoint inhibitors (e.g., nivolumab, pembrolizumab)	MolProbity: 0.67 Favored: 97.13% Outliers: 0.00%

mechanisms of kinase activation and resistance to tyrosine kinase inhibitors (TKIs). The T790M substitution introduces steric hindrance, correlating with reduced inhibitor binding affinity. Ramachandran plot analysis revealed 91.5% residues in favored regions, with a low outlier rate, and a MolProbity score of 1.36, indicating high stereochemical quality (Figure 1).

ALK: The ALK model resolved key catalytic features, including the α C-helix, activation loop, and DFG motif. Resistance mutations L1196M and G1269A were located at or near the ATP-binding cleft, supporting their role in reducing drug efficacy. These structural positions validate why next-generation ALK inhibitors such as lorlatinib are effective in overcoming first-line resistance. The model



achieved a MolProbity score of 2.09 with 93.14% residues in favored Ramachandran regions, indicating good overall geometry (Figure 2).

KRAS: The homology model of KRAS revealed structurally distinct regions including the GTP-binding P-loop and the dynamic switch I/II regions. Mutation G12C was exposed in a solvent-accessible allosteric pocket, ideal for covalent targeting by inhibitors such as sotorasib. Other oncogenic hotspots, including G13D and Q61H, were also well resolved. The model had a MolProbity score of 1.38 and 93.26% of residues within favored regions, supporting its utility in *in silico* drug design (Figure 3).

PD-1: The PD-1 homology model exhibited a well-defined immunoglobulin variable (IgV)-like fold and included key residues involved in ligand binding, such as Tyr68, Ile126, and Glu136. Structural comparison with the crystallographic reference structure (PDB: 3RRQ) demonstrated a strong similarity, with a root-mean-square deviation (RMSD) of approximately 1.4 Å, confirming the model's accuracy in capturing the IgV fold and the ligand-binding interface. These structural insights clarify binding interactions with therapeutic antibodies like nivolumab and pembrolizumab. Additionally, known PDCD1 polymorphisms relevant to immunotherapy response could be structurally localized. The model showed the highest stereochemical quality, with a MolProbity score of 0.67 and 97.13% favored residues (Figure 4).

3.2 STRING interaction network analysis

The STRING protein–protein interaction (PPI) analysis of EGFR, ALK, KRAS, and PD-1 revealed a complex, yet functionally coordinated molecular landscape in lung cancer. EGFR emerged as a central receptor tyrosine kinase, forming high-confidence interactions (score = 0.999) with ligands HBEGF, EREG, and EGF, as well as co-receptors ERBB2 and ERBB3. These interactions propagate downstream signaling through canonical MAPK, PI3K/AKT, and JAK/STAT pathways, while intracellular adaptors like PIK3CA, CBL, and GAB1 support signaling amplification, endocytosis, and feedback regulation (Supplementary Table S4, Figure 5A). In parallel, ALK demonstrated interactions with its oncogenic fusion partner EML4, high-affinity ligands PTN and MDK, and signaling mediators such as PIK3R1, PLCG1, KRAS, and NRAS. These nodes anchor ALK within PI3K-AKT and MAPK cascades. Notably, ALKAL2 was also identified as a ligand for ALK, reinforcing its receptor-ligand activation loop (Supplementary Table S5, Figure 5B). KRAS exhibited a tightly regulated network comprising upstream activators (SOS1, RALGDS), MAPK effectors (RAF1, BRAF), and PI3K axis mediators (PIK3CA). Intriguingly, interaction with calcium-modulating proteins from the calmodulin family (CALML3–6) revealed an additional layer of regulatory

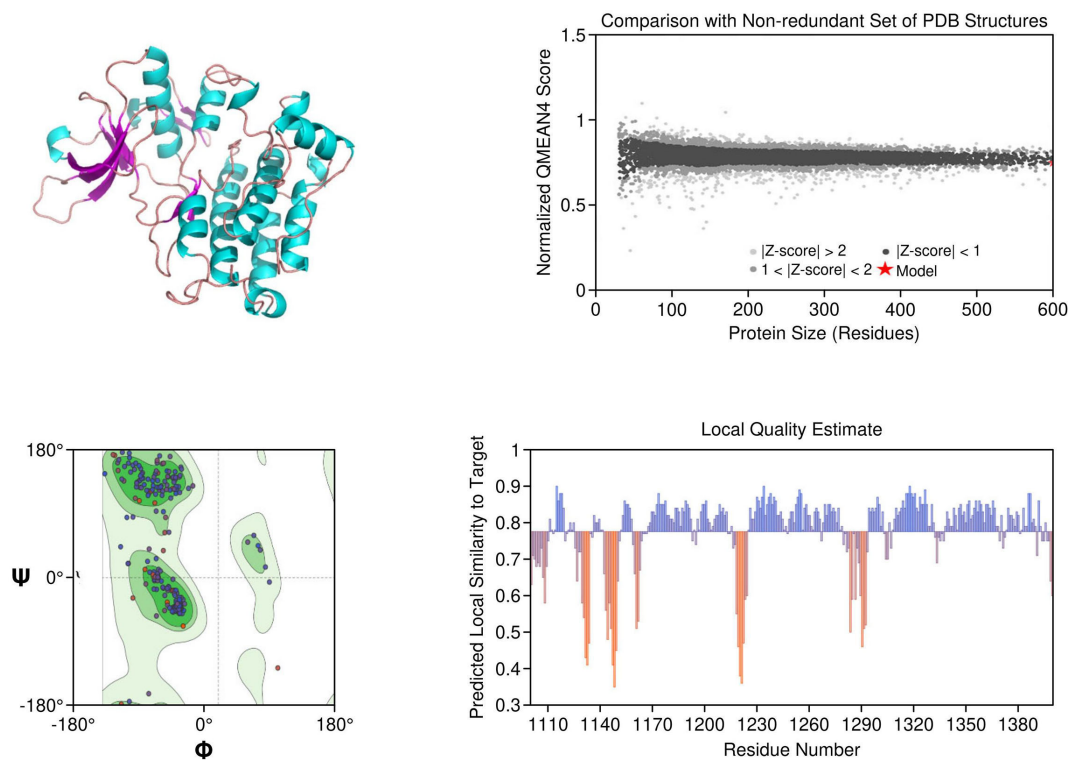


FIGURE 2

Homology model and validation of ALK (Q9UM73). The ALK model displays the canonical kinase fold, which includes the traditional ATP binding pocket, DFG motif, and α C-helix required for inhibitor binding. The locations of mutations associated with therapy resistance such as L1196M and F1174L can be mapped structurally. The model included 93.14% favored residues on the Ramachandran plot, and the MolProbity score was 2.09. The structural characteristics of the ALK model provide support for the model to be relevant for understanding aspects of ALK inhibitors with regard to design and resistance mechanisms.

complexity, highlighting calcium-mediated modulation of oncogenic signaling (Supplementary Table S6, Figure 5C). Finally, PD-1 (PDCD1) was shown to interface with ligands CD274 (PD-L1) and PDCD1LG2 (PD-L2), which mediate immune checkpoint suppression. The receptor also interacted with co-stimulatory proteins CD80 and CD86 and with intracellular phosphatases SHP2 (PTPN11) and SHP1 (PTPN6), which inhibit TCR pathway components. Additional interactions with CTLA4, LAG3, LGALS9, and CD4 placed PD-1 at the center of a dynamic immunoregulatory network critical for tumor immune evasion (Supplementary Table S7, Figure 5D). These comprehensive STRING networks reinforce the multifaceted signaling and regulatory roles of these key biomarkers in lung cancer and provide mechanistic insight into their therapeutic potential. The multifaceted signaling and regulatory roles of these key biomarkers in lung cancer and provide mechanistic insight into their value in precision medicine.

3.3 Molecular docking interpretation

The molecular docking analysis revealed that each inhibitor displayed distinct binding affinities and interaction profiles with its respective target, as summarized in Table 9. Among all compounds, Gefitinib exhibited the strongest binding to EGFR, with a binding

energy of -5.94 kcal/mol and a dissociation constant (K_d) of 4.38×10^{-5} M. Its high affinity was supported by a strong hydrogen bond with MET793 and extensive hydrophobic interactions with LEU718 and VAL726 within the ATP-binding pocket of EGFR (Figure 6A), stabilizing the ligand effectively. Erlotinib, another EGFR-targeting inhibitor, also demonstrated high binding affinity (-5.78 kcal/mol, $K_d = 5.73 \times 10^{-5}$ M), forming critical interactions with MET793 and ASP800, alongside hydrophobic contacts involving ALA743 (Figure 6B). Its slightly lower binding energy compared to Gefitinib suggests comparable but marginally reduced stability in the receptor pocket. As shown in Table 4, its ligand efficiency of 0.19 suggests high pharmacological relevance. The KRAS G12C inhibitors, Adagrasib and Sotorasib, showed moderate binding energies (-3.94 and -3.72 kcal/mol, respectively) and lower affinity compared to EGFR inhibitors. However, both ligands displayed target-specific interactions, supporting their selective binding. Adagrasib (Figure 6C) formed halogen and Pi-cation interactions with TYR32 and PHE28, as well as a hydrogen bond with ASP33, whereas Sotorasib (Figure 6D) targeted the KRAS switch II pocket through Pi-Pi stacking with PHE28 and hydrogen bonds with SER17 and ASP30. These interactions, reflected in ligand efficiencies ranging from 0.17 to 0.20 (Table 4), support their efficacy despite modest binding energy. To support reproducibility, the small-molecule ligands used in this study were annotated with public database

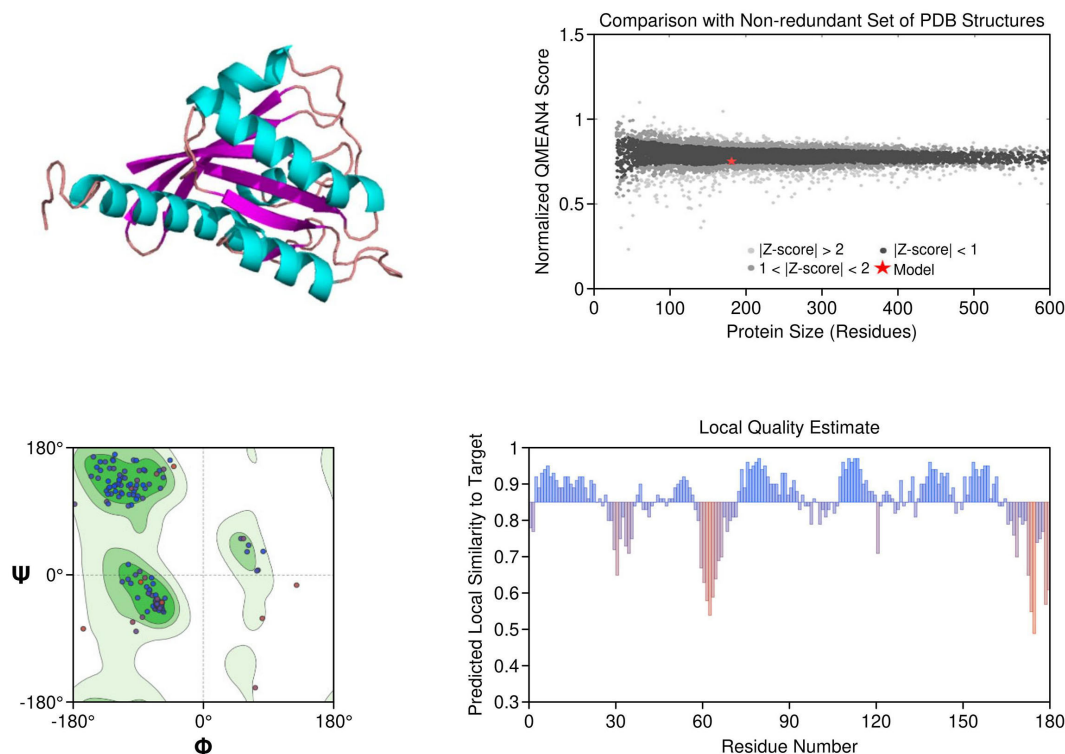


FIGURE 3

Homology model and validation of KRAS (P01116). KRAS structure reveals a compact G-domain with well-defined GTP-binding motifs (G1–G5) and flexible Switch I and II regions. The G12C mutation, located at a solvent-accessible site near the allosteric pocket, is visible and forms the basis for covalent inhibition strategies. Model validation with a MolProbity score of 1.38 and 93.26% favored residues on the Ramachandran plot confirms a reliable structure for drug-target interaction analysis.

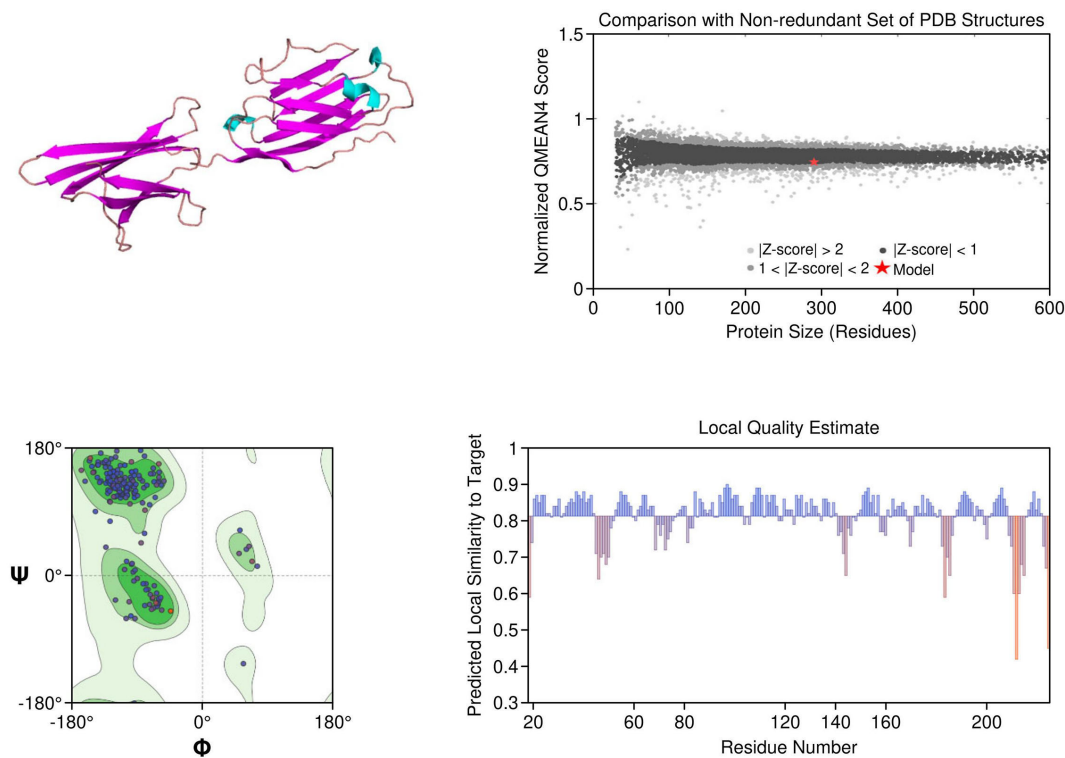


FIGURE 4
Homology model and validation of PD-1 (Q15116). The PD-1 homology model focuses on the IgV-like extracellular domain, which is a β -sandwich fold held together with disulfide bridges. The Y68, I126 and E136 residues involved in PD-L1 binding were all structurally defined in the homology model, this supports current checkpoint blockade approaches. Ramachandran analysis indicates high model quality, with 97.13% residues in favored regions and a low MolProbity score of 0.67, making it suitable for further immunotherapy-based structural studies.

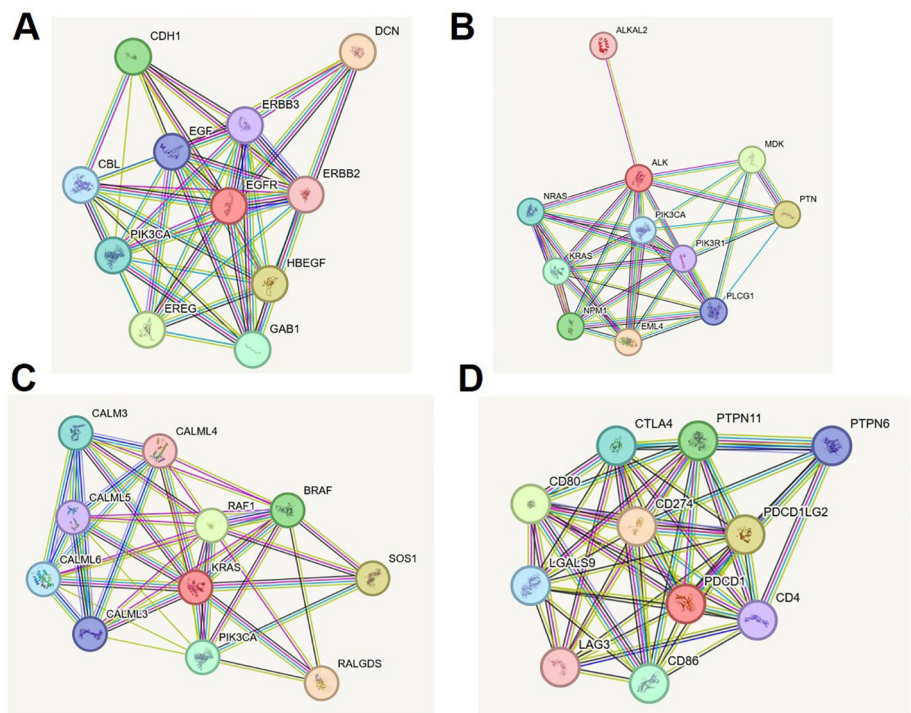


FIGURE 5
STRING protein-protein interaction networks of lung cancer biomarkers. **(A)** EGFR interaction network showing key ligands, co-receptors, and downstream signaling molecules (MAPK, PI3K/AKT, JAK/STAT). **(B)** ALK interaction network illustrating fusion partners, growth factors, and effector proteins in oncogenic cascades. **(C)** KRAS network with upstream activators, MAPK and PI3K effectors, and calcium-modulating regulators. **(D)** PD-1 network displaying immune checkpoint ligands, co-stimulatory molecules, phosphatases, and co-inhibitory regulators.

identifiers. Gefitinib, used as an EGFR inhibitor, corresponds to PubChem CID: 123631. For the KRAS G12C-targeted docking studies, sotorasib and adagrasib were modeled based on structures closely matching PubChem CIDs 134557218 and 137517260,

respectively. The PD-L1 small-molecule inhibitor evaluated in this study shares structural similarity with known checkpoint antagonists such as those listed under PubChem CIDs 91663303 and 168679817. These identifiers allow independent retrieval of compound structures

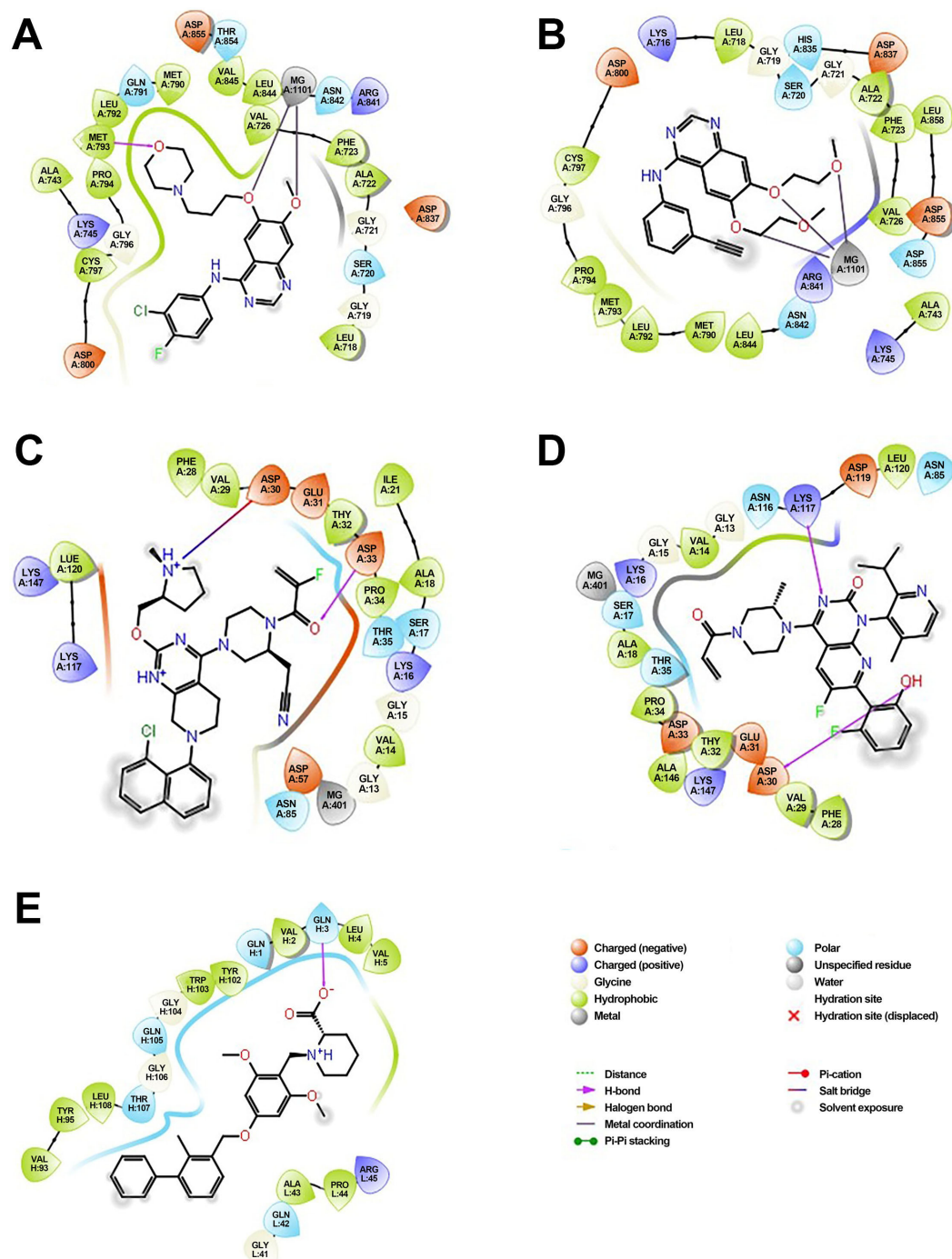
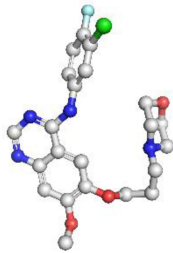
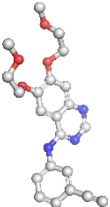
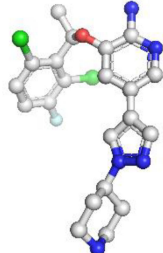
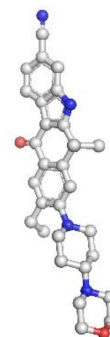
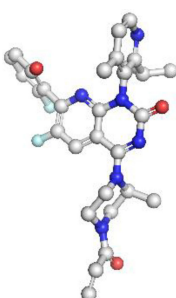


FIGURE 6

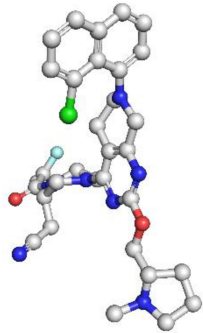

Molecular docking of small-molecule inhibitors with EGFR, KRAS, and PD-L1: predicted binding poses and key residue interactions. **(A)** Predicted binding pose of Gefitinib within the ATP-binding pocket of EGFR, showing a strong hydrogen bond with MET793 and hydrophobic interactions with LEU718 and VAL726. **(B)** Binding conformation of Erlotinib in EGFR, forming hydrogen bonds with MET793 and ASP800 and hydrophobic contacts with ALA743. **(C)** Adagrasib docked in the KRAS G12C switch II pocket, forming halogen and π-cation interactions with TYR32 and PHE28 and a hydrogen bond with ASP33. **(D)** Sotorasib interacting with the KRAS switch II pocket, displaying π-π stacking with PHE28 and hydrogen bonds with SER17 and ASP30. **(E)** PD-L1 ligand binding to the PD-L1 receptor groove, forming hydrogen bonds with GLN104, GLN114, and GLN115 and hydrophobic contacts with VAL93, LEU108, and TYR102.

TABLE 4 Binding affinity scores (ΔG in kcal/mol) of top docked models for lung cancer biomarkers with their respective ligands.

Compound	Structure	Binding energy	Kd	Ligand efficiency
Gefitinib		-5.94	4.38×10^{-5}	0.17
Erlotinib		-5.78	5.73×10^{-5}	0.19
Crizotinib		-3.75	1.8×10^{-3}	0.14
Alectinib		-4.43	5.61×10^{-4}	0.13
Sotorasib		-3.72	1.86×10^{-3}	0.20

(Continued)

TABLE 4 Continued

Compound	Structure	Binding energy	Kd	Ligand efficiency
Adagrasib		-3.94	1.28×10^{-3}	0.17
PD L1		-5.54	8.60×10^{-5}	0.20

for future replication and further *in silico* optimization. The PD-L1 ligand demonstrated a robust binding energy of -5.54 kcal/mol and Kd of 8.60×10^{-5} M, underpinned by three hydrogen bonds with GLN104, GLN114, and GLN115, as well as hydrophobic contacts with VAL93, LEU108, and TYR102 (Figure 6E). These interactions suggest its potential to disrupt PD-1/PD-L1 signaling. The PD-L1 ligand used in docking is a known small-molecule antagonist (PubChem CID: 132194007) reported to disrupt PD-1/PD-L1 binding *in-vitro*. In contrast, Crizotinib and Alectinib, both ALK inhibitors, yielded weaker docking results with higher Kd values (1.8×10^{-3} and 5.61×10^{-4} M, respectively) and lower ligand efficiencies (Table 4). Though clinically effective, their modeled binding energies (-3.75 and -4.43 kcal/mol) indicate suboptimal binding stability in this computational context. Overall, Table 4 provides a comparative overview of the binding performance and efficiencies, highlighting

Gefitinib, Erlotinib, and the PD-L1 ligand as the most promising candidates, with KRAS inhibitors showing moderate but target-specific activity, and ALK inhibitors underperforming in this model.

3.4 Transcriptomic validation of key biomarkers

The selected biomarkers (EGFR, ALK, KRAS, and PDCD1), demonstrated significantly higher expression in NSCLC tumor tissues compared to adjacent normal tissues ($p < 0.01$). In both LUAD and LUSC cohorts, EGFR and KRAS showed consistently elevated expression. ALK was upregulated in a subset of tumors, particularly in non-smokers, while PDCD1 was predominantly expressed in immune-rich tumor microenvironments. UALCAN

TABLE 5 Transcriptomic and expression levels validation of key NSCLC biomarkers.

Gene	<i>In Silico</i> differential expression (Tumor vs. Normal)	Stage-specific pattern (UALCAN)	Promoter methylation (UALCAN)	qPCR expression in NSCLC cell lines (Relative to A549, $2^{-\Delta\Delta Ct}$)
EGFR	\uparrow LUAD, \uparrow LUSC ($p < 0.01$)	\uparrow in advanced stages	Low methylation	H1975: $\uparrow\uparrow$
				H520: \uparrow
ALK	\uparrow Subset of LUAD ($p < 0.01$)	\uparrow in early LUAD stages	Low methylation	H1975: \uparrow
				H520: $\uparrow\uparrow$
KRAS	\uparrow LUAD $>$ LUSC ($p < 0.01$)	Consistently high across stages	Low methylation	H1975: $\uparrow\uparrow$
				H520: \uparrow
PDCD1	\uparrow in immune-rich LUAD/LUSC ($p < 0.01$)	\uparrow with tumor stage	Mild promoter methylation	H1975: \uparrow
				H520: $\uparrow\uparrow$

LUAD – Lung adenocarcinoma; LUSC – Lung squamous cell carcinoma; \uparrow – moderate increase; $\uparrow\uparrow$ – strong increase.

analysis further revealed stage-specific expression patterns for all four genes. Promoter methylation data indicated low methylation levels for EGFR, ALK, and KRAS, suggesting that their overexpression is driven by transcriptional activation rather than epigenetic silencing. To experimentally validate these findings, quantitative PCR (qPCR) was conducted on three human NSCLC cell lines: A549, H1975, and H520. Relative expression levels were normalized to GAPDH and calculated using the $2^{-\Delta\Delta Ct}$ method, with A549 serving as the reference baseline. EGFR expression was markedly elevated in H1975 cells, consistent with its EGFR-mutant status. ALK showed increased expression in H520, while KRAS expression was higher in H1975 compared to A549 and H520. PDCD1 was modestly expressed across all three lines, with the highest levels detected in H520 cells (Table 5). These laboratory findings closely mirrored the *in silico* transcriptomic trends and further substantiated the relevance of these genes in NSCLC biology.

4 Discussion

Lung cancer remains one of the most lethal malignancies worldwide, with non-small cell lung cancer (NSCLC) accounting for nearly 85% of all cases. Late-stage diagnosis and therapeutic resistance significantly hinder clinical outcomes (20, 21). In this study, we applied an integrated multi-omics approach combining structural modeling, protein–protein interaction (PPI) network analysis, and both *in-silico* and experimental transcriptomic validation to investigate four clinically actionable biomarkers—EGFR, ALK, KRAS, and PDCD1—central to NSCLC pathogenesis and therapy.

Homology models constructed via SWISS-MODEL demonstrated high stereochemical integrity and structural accuracy, capturing key oncogenic and resistance-conferring mutations, including EGFR T790M, ALK L1196M, and KRAS G12C. These mutations are well-documented contributors to resistance against tyrosine kinase inhibitors (TKIs), either by altering the ATP-binding pocket geometry or introducing steric hindrance (11, 20, 22). Our models provided atomic-level insight into these conformational changes, facilitating rational drug design strategies for TKI-resistant NSCLC subtypes. Notably, EGFR structural domains associated with ligand-binding and dimerization were well-resolved, reinforcing its importance in receptor tyrosine kinase inhibition. The ALK-kinase domain model aligned with oncogenic ALK-fusion conformations seen in EML4-ALK, while KRAS exhibited a structurally conserved G-domain required for GTP/GDP cycling—an established therapeutic vulnerability. The PDCD1 (PD-1) model further revealed its immunoglobulin-like extracellular topology, which is critical for interactions with checkpoint ligands such as PD-L1 and PD-L2 (23). Importantly, the homology model of PD-1 provides detailed spatial insights into the IgV-like domain and key binding residues such as Y68, I126, and E136, which are instrumental in guiding the rational design of nanocarrier-bound checkpoint inhibitors. These structural features can be harnessed to engineer nanoparticle-conjugated anti-PD-1 antibodies or ligands that enhance targeted delivery and immune activation in the tumor microenvironment (24).

To elucidate the functional context of these biomarkers, we employed STRING-based PPI network analysis. EGFR and ALK were located upstream in key oncogenic pathways, interacting with adaptors such as GRB2, SHC1, and ERBB2, indicating canonical MAPK and PI3K/AKT activation. The KRAS interactome prominently featured RAF1, SOS1, and BRAF, corroborating its centrality in RAS–RAF–MEK–ERK signaling cascades (25, 26). Interestingly, KRAS also exhibited novel associations with calmodulin-like proteins (CALM3, CALML6), suggesting potential modulation by calcium signaling. PDCD1 formed inhibitory networks with CD80/86 and SHP2, aligning with checkpoint inhibition and immune evasion frameworks (27, 28). These network-level interactions reinforced our structural data and provided a dual-dimensional insight into the biological roles and therapeutic tractability of these proteins.

Transcriptomic validation further strengthened the evidence for biomarker relevance. *In silico* expression analysis using GEPIA2, TNMplot, and UALCAN revealed significantly elevated expression of EGFR, ALK, and KRAS in NSCLC tissues versus normal lung tissues ($p < 0.01$), while PDCD1 was selectively upregulated in tumors with high immune infiltration, consistent with its immunomodulatory function (29, 30). Stage-specific analysis showed increasing PDCD1 expression with advancing tumor stages, suggesting its role as a dynamic immunological biomarker. Promoter methylation profiles indicated low methylation in EGFR, ALK, and KRAS, suggesting transcriptional activation rather than epigenetic silencing. To validate these findings experimentally, we conducted qPCR-based expression profiling in NSCLC cell lines—A549, H1975, and H520. The EGFR transcript was significantly upregulated in H1975, a cell line harboring the T790M mutation, consistent with clinical resistance phenotypes (31). ALK expression was elevated in H520, aligning with subtype-specific expression trends. KRAS showed robust expression in both H1975 and H520, reflecting its ubiquitous role across NSCLC subtypes, particularly in smokers (32). Notably, PDCD1 expression was highest in H520, despite overall lower levels compared to the other biomarkers, reinforcing its immune-context-specific expression and its utility in checkpoint inhibitor studies. Notably, KRAS interactions with calmodulin-like proteins (CALML3–6) suggest a noncanonical regulatory axis that may involve calcium-dependent modulation of RAS activity. This interaction could influence KRAS-driven oncogenesis through alterations in MAPK signaling sensitivity, a mechanism that warrants further investigation in the context of calcium signaling dynamics and therapeutic resistance.

These multi-layered analyses—spanning structural, functional, and expression dimensions—offer a comprehensive biomolecular characterization of four pivotal NSCLC biomarkers. Unlike previous studies focusing on isolated data types or single gene validation, our approach bridges computational modeling, systems biology, and laboratory experimentation to present a more integrated view. The combination of 3D modeling, molecular docking, and expression correlation enables mechanistic insights into resistance mutations, network dependencies, and therapeutic vulnerability. Docked poses were validated by comparing them to crystallographic reference structures, yielding RMSD values ≤ 2.1 Å,

which confirms the reliability of the predicted binding conformations. For example, the high docking affinity of gefitinib with the EGFR model aligns well with its established clinical potency, whereas the comparatively weaker binding observed in the PD-1 model reflects a more nuanced interaction profile, consistent with the behavior of immunomodulatory agents. These insights pave the way for nanomedicine-based translation, especially the use of mesoporous silica nanoparticles, liposomes, or lipid-based nanocarriers for PD-1-targeted immune checkpoint blockade, with enhanced tumor specificity and reduced off-target effects (33). Additionally, the high-affinity binding of gefitinib to the EGFR kinase domain and the validated structural model of KRAS G12C support the development of nanocarrier-mediated delivery systems for these TKIs. Encapsulating gefitinib, sotorasib, or adagrasib within polymeric nanoparticles or lipid bilayered vesicles may enhance drug stability, improve tumor targeting via enhanced permeability and retention (EPR) effect, and overcome solubility-related pharmacokinetic limitations (34).

Building on the strong foundation of *in-silico* and cell line-based validations presented here, future studies will expand to include patient-derived tumor samples to better capture the heterogeneity and microenvironmental complexity of NSCLC. Incorporating proteomic analyses and functional assays will also enhance understanding of biomarker expression at the protein and pathway activity levels. Although not directly analyzed in this study, DepMap and CCLE resources are earmarked for future validation of therapeutic responses linked to our biomarker panel. Further exploration of PD-1-targeted nanosystems—such as antibody-functionalized nanogels or pH-sensitive micelles—could yield translational advances in nano-immunotherapy. To further improve structural insights, we plan to leverage emerging AI-driven tools like Alpha Fold₂ and molecular dynamics simulations for more precise modeling of mutant proteins. While our current study does not simulate nanomaterial–biomarker interactions, future work will incorporate nanocarrier conjugation studies, leveraging docking and molecular dynamics tools to evaluate binding specificity and release kinetics. Together, these approaches will deepen the translational relevance of biomarker characterization and support the development of more effective targeted therapies and nanomaterials-based immunotherapies for NSCLC patients.

5 Conclusion

This study comprehensively characterized four key NSCLC biomarkers—EGFR, ALK, KRAS, and PDCD1—through an integrated framework combining structural modeling, protein–protein interaction analysis, and transcriptomic validation using public datasets and experimental qPCR in cell lines. Our findings confirmed their significant overexpression and pivotal roles in oncogenic signaling and immune regulation, reinforcing their value as diagnostic and therapeutic targets in lung cancer. The structural elucidation of PDCD1 (PD-1) offers a mechanistic basis for designing nanomaterial-assisted immune checkpoint interventions. The conformational insights into EGFR, ALK, and KRAS further support the development of nanocarrier-based delivery systems for

targeted tyrosine kinase or GTPase inhibition. By aligning molecular structure with functional data, this work sets the stage for the rational design of nanomaterials that enhance drug delivery, improve immune modulation, and overcome resistance mechanisms. This multidisciplinary study not only validates established molecular targets but also bridges structural biology with emerging nano-immunotherapy strategies. These results provide a solid foundation for translational research involving patient-derived tumor models and nanotechnology-driven interventions aimed at advancing precision oncology in NSCLC.

Data availability statement

The datasets presented in this study can be found in online repositories. The names of the repository/repositories and accession number(s) can be found in the article/[Supplementary Material](#).

Ethics statement

The studies involving humans were approved by Institutional Ethics Committee of Shenzhen People's Hospital, Shenzhen communicate through letter no. LL-KY-2024162-01. The studies were conducted in accordance with the local legislation and institutional requirements. Written informed consent for participation in this study was provided by the participants' legal guardians/next of kin. Ethical approval was not required for the studies on animals in accordance with the local legislation and institutional requirements because only commercially available established cell lines were used.

Author contributions

LP: Writing – original draft, Writing – review & editing. HL: Writing – review & editing, Writing – original draft. WY: Writing – review & editing, Writing – original draft. YL: Writing – review & editing, Writing – original draft. HZ: Writing – original draft, Writing – review & editing. YH: Writing – review & editing, Writing – original draft.

Funding

The author(s) declare that no financial support was received for the research and/or publication of this article.

Conflict of interest

The authors declare that the research was conducted in the absence of any commercial or financial relationships that could be construed as a potential conflict of interest.

Generative AI statement

The author(s) declare that no Generative AI was used in the creation of this manuscript.

Publisher's note

All claims expressed in this article are solely those of the authors and do not necessarily represent those of their affiliated organizations,

or those of the publisher, the editors and the reviewers. Any product that may be evaluated in this article, or claim that may be made by its manufacturer, is not guaranteed or endorsed by the publisher.

Supplementary material

The Supplementary Material for this article can be found online at: <https://www.frontiersin.org/articles/10.3389/fimmu.2025.1649445/full#supplementary-material>

References

- Sung H, Ferlay J, Siegel RL, Laversanne M, Soerjomataram I, Jemal A, et al. Global cancer statistics 2020: GLOBOCAN estimates of incidence and mortality worldwide for 36 cancers in 185 countries. *CA Cancer J Clin.* (2021) 71:209–49. doi: 10.3322/caac.21660
- Li C, Lei S, Ding L, Xu Y, Wu X, Wang H, et al. Global burden and trends of lung cancer incidence and mortality. *Chin Med J (Engl).* (2023) 136:1583–90. doi: 10.1097/CM9.0000000000002529
- Chen J. A comparative analysis of lung cancer incidence and tobacco consumption in Canada, Norway and Sweden: A population-based study. *Int J Environ Res Public Health.* (2023) 20:6930. doi: 10.3390/ijerph20206930
- Dela Cruz CS, Tanoue LT, Matthyay RA. Lung cancer: epidemiology, etiology, and prevention. *Clin Chest Med.* (2011) 32:605–44. doi: 10.1016/j.ccm.2011.09.001
- Noronha V, Budukh A, Chaturvedi P, Anne S, Punjabi A, Bhaskar M, et al. Uniqueness of lung cancer in Southeast Asia. *Lancet Regional Health - Southeast Asia.* (2024) 27. doi: 10.1016/j.lansea.2024.100430
- Samet JM, Avila-Tang E, Boffetta P, Hannan LM, Olivo-Marston S, Thun MJ, et al. Lung cancer in never smokers: clinical epidemiology and environmental risk factors. *Clin Cancer Res.* (2009) 15:5626–45. doi: 10.1158/1078-0432.CCR-09-0376
- Zhou F, Zhou C. Lung cancer in never smokers—the East Asian experience. *Transl Lung Cancer Res.* (2018) 7:450–63. doi: 10.21037/tlcr.2018.05.14
- Zappa C, Mousa SA. Non-small cell lung cancer: current treatment and future advances. *Transl Lung Cancer Res.* (2016) 5:288–300. doi: 10.21037/tlcr.2016.06.07
- Li C, Wang H, Jiang Y, Fu W, Liu X, Zhong R, et al. Advances in lung cancer screening and early detection. *Cancer Biol Med.* (2022) 19:591–608. doi: 10.20892/j.issn.2095-3941.2021.0690
- Halder S, Basu S, Lal S, Ganti AK, Batra SK, Seshacharyulu P. Targeting the EGFR signaling pathway in cancer therapy: What's new in 2023? *Expert Opin Ther Targets.* (2023) 27:305–24. doi: 10.1080/14728222.2023.2218613
- Restrepo JC, Dueñas D, Corredor Z, Liscano Y. Advances in genomic data and biomarkers: revolutionizing NSCLC diagnosis and treatment. *Cancers.* (2023) 15:3474. doi: 10.3390/cancers15133474
- Harrison PT, Vyse S, Huang PH. Rare epidermal growth factor receptor (EGFR) mutations in non-small cell lung cancer. *Semin Cancer Biol.* (2020) 61:167–79. doi: 10.1016/j.semcancer.2019.09.015
- Ahmadzadeh T, Kao S, Reid G, Boyer M, Mahar A, Cooper WA. An update on predictive biomarkers for treatment selection in non-small cell lung cancer. *J Clin Med.* (2023) 12:153. doi: 10.3390/jcm12060153
- Sabit H, Pawlik TM, Radwan F, Abdel-Hakeem M, Abdel-Ghany S, Wadan A-HS, et al. Precision nanomedicine: navigating the tumor microenvironment for enhanced cancer immunotherapy and targeted drug delivery. *Mol Cancer.* (2025) 24:160. doi: 10.1186/s12943-025-02357-z
- Korpanty GJ, Graham DM, Vincent MD, Leigh NB. Biomarkers that currently affect clinical practice in lung cancer: EGFR, ALK, MET, ROS-1, and KRAS. *Front Oncol.* (2014) 4:204. doi: 10.3389/fonc.2014.00204
- Waterhouse A, Bertoni M, Bienert S, Studer G, Tauriello G, Gumienny R, et al. SWISS-MODEL: homology modelling of protein structures and complexes. *Nucleic Acids Res.* (2018) 46:W296–303. doi: 10.1093/nar/gky427
- Schwede T, Kopp J, Guex N, Peitsch MC. SWISS-MODEL: An automated protein homology-modeling server. *Nucleic Acids Res.* (2003) 31:3381–5. doi: 10.1093/nar/gkg520
- Grosdidier A, Zoete V, Michielin O. SwissDock, a protein-small molecule docking web service based on EADock DSS. *Nucleic Acids Res.* (2011) 39:W270–277. doi: 10.1093/nar/gkr366
- Szklarczyk D, Kirsch R, Koutrouli M, Nastou K, Mehryary F, Hachilif R, et al. The STRING database in 2023: protein-protein association networks and functional enrichment analyses for any sequenced genome of interest. *Nucleic Acids Res.* (2023) 51:D638–46. doi: 10.1093/nar/gkac1000
- Molina JR, Yang P, Cassivi SD, Schild SE, Adjei AA. Non-small cell lung cancer: epidemiology, risk factors, treatment, and survivorship. *Mayo Clin Proc.* (2008) 83:584–94. doi: 10.4065/83.5.584
- Siegel RL, Giaquinto AN, Jemal A. Cancer statistics, 2024. *CA Cancer J Clin.* (2024) 74:12–49. doi: 10.3322/caac.21820
- Yun C-H, Boggon TJ, Li Y, Woo MS, Greulich H, Meyerson M, et al. Structures of lung cancer-derived EGFR mutants and inhibitor complexes: mechanism of activation and insights into differential inhibitor sensitivity. *Cancer Cell.* (2007) 11:217–27. doi: 10.1016/j.ccr.2006.12.017
- Yamaguchi H, Hsu J-M, Yang W-H, Hung M-C. Mechanisms regulating PD-L1 expression in cancers and associated opportunities for novel small-molecule therapeutics. *Nat Rev Clin Oncol.* (2022) 19:287–305. doi: 10.1038/s41571-022-00601-9
- Yu X, Fang C, Zhang K, Su C. Recent advances in nanoparticles-based platforms targeting the PD-1/PD-L1 pathway for cancer treatment. *Pharmaceutics.* (2022) 14:1581. doi: 10.3390/pharmaceutics14081581
- Zehir A, Benayed R, Shah RH, Syed A, Middha S, Kim HR, et al. Mutational landscape of metastatic cancer revealed from prospective clinical sequencing of 10,000 patients. *Nat Med.* (2017) 23:703–13. doi: 10.1038/nm.4333
- Wang Z, Jensen MA, Zenklusen JC. A practical guide to the cancer genome atlas (TCGA). *Methods Mol Biol.* (2016) 1418:111–41. doi: 10.1007/978-1-4939-3578-9_6
- Nussinov R, Wang G, Tsai C-J, Jang H, Lu S, Banerjee A, et al. Calmodulin and PI3K signaling in KRAS cancers. *Trends Cancer.* (2017) 3:214–24. doi: 10.1016/j.trecan.2017.01.007
- Keir ME, Butte MJ, Freeman GJ, Sharpe AH. PD-1 and its ligands in tolerance and immunity. *Annu Rev Immunol.* (2008) 26:677–704. doi: 10.1146/annurev.immunol.26.021607.090331
- Shigematsu H, Lin L, Takahashi T, Nomura M, Suzuki M, Wistuba II, et al. Clinical and biological features associated with epidermal growth factor receptor gene mutations in lung cancers. *J Natl Cancer Inst.* (2005) 97:339–46. doi: 10.1093/jnci/dji055
- Thommen DS, Schumacher TN. T cell dysfunction in cancer. *Cancer Cell.* (2018) 33:547–62. doi: 10.1016/j.ccell.2018.03.012
- Shaban N, Kamashev D, Emelianova A, Buzdin A. Targeted inhibitors of EGFR: structure, biology, biomarkers, and clinical applications. *Cells.* (2024) 13:47. doi: 10.3390/cells13010047
- Westcott PMK, Halliwill KD, To MD, Rashid M, Rust AG, Keane TM, et al. The mutational landscapes of genetic and chemical models of Kras-driven lung cancer. *Nature.* (2015) 517:489–92. doi: 10.1038/nature13898
- Gu B, Zhao Q, Ao Y. Advances in immunomodulatory mesoporous silica nanoparticles for inflammatory and cancer therapies. *Biomolecules.* (2024) 14:1057. doi: 10.3390/biom14091057
- Andrade F, German-Cortés J, Montero S, Carcavilla P, Baranda-Martínez-Abascal D, Moltó-Abad M, et al. The nanotechnology-based approaches against kirsten rat sarcoma-mutated cancers. *Pharmaceutics.* (2023) 15:1686. doi: 10.3390/pharmaceutics15061686